Reaction Kinetics of Liquid Organic Hydrogen Carriers from First-Principles: The Methylcyclohexane/Toluene Pair on Pt(111)

ACS Catalysis

pubs.acs.org/acscatalysis
Research Article

Reaction Kinetics of Liquid Organic Hydrogen Carriers from First-Principles: The Methylcyclohexane/Toluene Pair on Pt(111)

Alvaro Posada-Borbón,* Tobias Möslinger, and Henrik Grönbeck*

Cite This: ACS Catal. 2026, 16, 12123−12134
Read Online

ABSTRACT: The use of hydrogen as an energy carrier relies on efficient storage technologies. One appealing alternative is liquid organic hydrogen carriers (LOHC), where hydrogen is stored in liquid organic molecules at standard conditions. Catalysts are used to facilitate the loading and unloading of hydrogen in the organic molecule and one example is the storage of three hydrogen molecules in toluene (C_7H_8), forming methylcyclohexane (C_7H_{14}). We have used density functional theory (DFT) calculations in combination with mean-field microkinetic modeling to understand the factors controlling the activity and selectivity of Pt(111) as a catalyst for the toluene/methylcyclohexane LOHC pair. The simulated temperature dependence of turnover frequencies, reaction orders, and apparent activation energies is in agreement with experimental trends, and the rate controlling steps are identified. A sensitivity analysis reveals that stabilization of methylcyclohexane adsorption is one potential way to improve the rate of dehydrogenation. The unwanted side reaction of hydrodemethylation of toluene to benzene is not relevant on Pt(111); however, the simulations indicate that the presence of undercoordinated Pt-sites will make this pathway an issue.

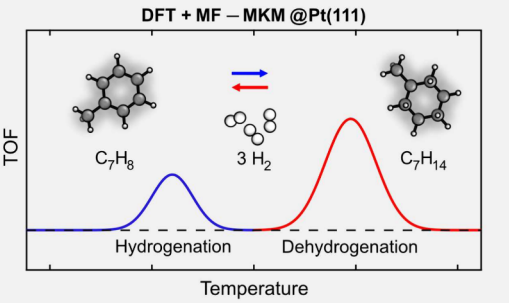

KEYWORDS: *density functional theory, microkinetic modeling, LOHC, Pt(111), methylcyclohexane, toluene*

INTRODUCTION

Hydrogen production from water splitting is one potential way to produce a fuel that is free of greenhouse gas emissions. However, the gaseous state of H_2 at standard conditions means that either high pressures (∼700 bar) or low temperatures (∼20 K) are required to store H_2, which limits the applicability of H_2 as an energy carrier. An alternative for hydrogen storage at standard conditions is based on loading and unloading of H_2 in organic molecules that are liquid at room temperature, so-called liquid organic hydrogen carriers (LOHC).[1−4] The loading/unloading is facilitated by catalytic hydrogenation/dehydrogenation. Two organic molecules that have been identified as a promising LOHC pair are toluene and methylcyclohexane (MCH). The molecules are stable at the reaction conditions, their toxicity is relatively low, and their gravimetric and volumetric hydrogen density is fairly high (6.2 wt % H_2 and energy density of 1.6 kWh/L).[5−10]

The catalytic hydrogenation/dehydrogenation of MCH and toluene is commonly performed over Pt-based catalysts.[11−20] Despite substantial experimental reports, mainly on the dehydrogenation reactions, a coherent understanding of the reaction kinetics is lacking. Sinfelt et al.[11] measured MCH dehydrogenation over a Pt/Al_2O_3 catalyst to be zero-order in MCH at near-ambient pressures (1.47−6.39 bar) in a temperature range 589−645 K, and the rate was suggested to be controlled by the desorption of toluene.[11] Van Trimpont et al.,[12] also reported a zero-order dependence of MCH in the dehydrogenation at pressures above 1.5 bar (582−683 K) over a sulfided Pt catalyst supported on Al_2O_3. A first-order dependence of MCH was, instead, measured at pressures below 0.5 bar. The rate-determining step was in ref 12. reported to be located close to the last dehydrogenation steps $C_7H_{10} \rightarrow C_7H_8$. Nagatake et al.[15] reported a slightly negative reaction order (−0.14) of toluene during the dehydrogenation of MCH over Pt/Al_2O_3; thus, toluene was found to inhibit the reaction. The reaction was in this case performed at 0.2 bar, and the reaction order in MCH was 0.8.[15] Most recently, Chen et al.[16] investigated the effect of particle size on the dehydrogenation of Pt/Al_2O_3, observing an optimal size of 1.57 nm. The optimal size was explained as a balance between the presence of active sites and the strength of toluene adsorption.[16]

Different theoretical models for the dehydrogenation of MCH over Pt were investigated and compared to experiments by Alhumaidan et al.[13] A model where the hydrogen coverage

Received: February 23, 2026
Revised: May 25, 2026
Accepted: May 26, 2026
Published: June 21, 2026

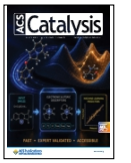

https://doi.org/10.1021/acscatal.6c01477
ACS Catal. 2026, 16, 12123−12134

depends non-linearly on pressure, the reactants do not compete for sites, and the dehydrogenation occurs sequentially in a stepwise fashion was found to best describe the measured kinetics.[13] The reaction orders were close to zero for both MCH and H_2 in a pressure range of 1−9 bar (613.15−723.15 K). The rate-controlling step was found to be close to the first dehydrogenation step.[13,14]

The reversed reaction, i.e., hydrogenation of toluene to MCH, has not been investigated to the same extent as the dehydrogenation reaction. Thus, while some phenomenological observations have been provided on the kinetics,[17,18] the elementary mechanisms, kinetic parameters, and rate-controlling steps are still undetermined. Thus, despite the numerous kinetic investigations, no unified understanding of the kinetic parameters controlling the reaction has been achieved.

Density functional theory (DFT) calculations of the MCH/toluene pair have provided information on adsorption and reaction energies.[21−24] Zhao et al.[21] stressed that van der Waals interactions are needed to describe the adsorption of the physisorbed molecules on Pt_{13}/Al_2O_3. The highest energy barrier for MCH dehydrogenation was found to be the $C_7H_{12} \rightarrow C_7H_{11} + H$ reaction step having a barrier of 0.99 eV.[21] Chen et al.[22] instead reported the $C_7H_{14} \rightarrow C_7H_{13} + H$ to have the highest barrier (1.41 eV) on Pt(111). More recently, Onyebuchi Obodo et al.[24] studied the effect of stepped surfaces [Pt(211) and Pt(311)] on the dehydrogenation of MCH to toluene.[24] A lower barrier for dehydrogenation was reported for the (311) surface, as compared to the (111) surface, suggesting the presence of step sites could improve the dehydrogenation rates.[24] To investigate the effect of surface alloying, Mi et al.[23] studied a Ni/Pt alloy supported on Pt(111).[23] The reaction intermediates were generally found to have lower adsorption energies on the surface alloy as compared to the bare Pt-system and the Pt-sites were identified as the active sites for the reactions. The decrease in adsorption energy on the Ni-containing system was explained as a result of electron transfer from Ni to the Pt. The first dehydrogenation step was in this study reported to have the highest barrier (2.16 eV).[23]

Although DFT investigations have provided important information on the C_7H_{14}/C_7H_8 system on Pt(111), a detailed mechanistic understanding that elucidates the rate control of the reaction, reaction orders, and the conditions controlling the competing hydrodemethylation reaction is still missing. In particular, a complete first-principles-based microkinetic investigation, considering both parts of the LOHC cycle, has, to the best of our knowledge, not been attempted previously. Here, we investigate the complete reaction mechanisms for the dehydrogenation of MCH to toluene and the hydrogenation of toluene to MCH, including the hydrodemethylation of toluene on Pt(111) using DFT-based mean-field microkinetic modeling. The predicted temperature dependence of the turnover frequency, reaction orders, and apparent activation energy elucidates experimental observations. The kinetic analysis shows that the dehydrogenation of MCH is controlled by the first two dehydrogenation steps and the desorption of MCH. Hydrogenation of toluene is controlled by the first and last hydrogenation steps and the desorption of toluene. Toluene hydrodemethylation is low on Pt(111) at relevant operating conditions. The rate-determining steps for this unwanted side reaction are the C−C scission and benzene desorption. The simulations reveal that stabilization of methylcyclohexane adsorption is one potential way to improve the dehydrogenation reaction rate, whereas destabilization of toluene adsorption is predicted to increase the rate of MCH dehydrogenation.

METHODS

DFT Calculations

Density functional theory (DFT) calculations are performed using the Vienna ab initio simulation package (VASP).[25−28] The Kohn−Sham orbitals are expanded with a plane wave basis, truncated at an energy of 450 eV. Interaction between the valence and core electrons is described with projector augmented wave potentials (PAW).[29,30] The explicitly treated valence electrons for hydrogen, carbon, and platinum are 1s, $2s^22p^2$, and $5d^96s^1$, respectively. The exchange correlation energy is calculated using the Perdew, Burke, Ernzerhof (PBE) formulation,[31] and van der Waals interactions are approximated with the Grimme-D3 method with zero damping.[32] The electronic structure is considered to be converged when the energy difference between electronic minimization steps is smaller than 10^{-6} eV. Structures are considered to be converged when the difference in forces acting on the atoms is smaller than 0.01 eV/Å. All reaction energies are calculated using the climbing-image nudged elastic band (CI-NEB) technique.[33] In general, a total of nine images is used along the reaction coordinate to describe the minimum energy path. A force criterion of 0.01 eV/Å is used for the transition state calculations. The existence of a saddle point in the potential energy surface is confirmed by vibrational analysis, where one imaginary frequency is found. All vibrational analyses are performed using finite differences with displacements of 0.015 Å.

Pt(111) is modeled with a $p(4 \times 4)$ surface cell, described with four layers, where the bottom two layers are constrained to their bulk positions for all optimizations. The slab models are separated from their repeating images by a vacuum of 20 Å in the z-direction. The surface cell is large enough to prevent repulsive interactions between periodic cells. The adsorption energy is within 0.03 eV lower in a $p(5 \times 5)$ surface cell for both toluene and MCH. Integration of the Brillouin zone is performed with finite sampling, centered at the gamma point, using a k-mesh of $4 \times 4 \times 1$. Energy calculations for the gas-phase species are performed in a $20 \times 21 \times 22$ Å^3 simulation box, ensuring a separation of at least 14 Å between repeating images. Spin-restricted calculations are performed unless otherwise stated. The structure model figures presented are generated with the software VESTA.[34]

Microkinetic Modeling

Kinetics of the reaction are investigated within the mean-field approximation. Thus, the rate of reaction for every elementary step is assumed to be proportional to the surface coverage of the reacting species

$$\frac{d\theta_i}{dt} = \sum_j c_{ij} r_j\left(\vec{\theta}\right) \quad (1)$$

θ_i is the coverage of species i, c_{ij} is the number of i molecules in reaction j, and $r_j(\vec{\theta})$ is the surface-coverage dependent reaction rate for reaction j. The set of coupled ordinary differential equations (ODEs) is integrated numerically as a function of time to obtain the steady state surface coverages at a given temperature

https://doi.org/10.1021/acscatal.6c01477
ACS Catal. 2026, 16, 12123−12134

and pressure. The integration of the ODEs is performed using the Scipy ODE solver for initial value problems with automatic selection between Adams/backward differentiation formula method.[35,36] Adsorbed cyclic carbon molecules occupy more than one Pt-site, and the maximum total coverage of these carbon intermediates is set to 0.11 ML. The limiting coverage is based on the DFT calculations and is consistent with experimentally observed limiting coverages.[37−39] Lateral interactions for the cyclic carbon intermediates are evaluated from the coverage-dependent adsorption energy of toluene. The coverage-dependent adsorption energy of toluene follows a sigmoid function:

$$E_{\text{ads}} = E^0_{ads} \times \left[1.02 - \left(\frac{0.3}{1+\exp\left(\frac{0.05-\sum_i \theta_i}{0.02}\right)}\right)\right] \tag{2}$$

E^0_{ads} is the adsorption energy in the dilute coverage limit, and $\sum_i \theta_i$ is the sum of the coverages for all cyclic carbon-based molecules. The same sigmoid function is used for the adsorption energies of all cyclic carbon molecules and hydrogenation/dehydrogenation steps. The applied lateral interactions for the cyclic carbon molecules are similar to the interactions measured for benzene[38] and naphthalene.[39] A linear function is used to account for the coverage dependence of the hydrogen adsorption energy:

$$E_{\text{ads},H} = E^0_{\text{ads},H} - 0.1 \cdot \theta_H \tag{3}$$

$E^0_{\text{ads},H}$ is the adsorption energy in the dilute limit.

The rate constants for unactivated adsorption (k_i^{ads}) are calculated from kinetic gas theory:[40]

$$k_i^{ads} = \frac{p_i A_{site}}{\sqrt{2\pi m_i k_B T}} \tag{4}$$

Here, the subscript i refers to the adsorbing species and p_i is its partial gas-phase pressure. A_{site} is the surface area of an adsorption site, set to 10 Å^2, m_i is the molecular mass of the adsorbate, k_B is Boltzmann's constant, and T is the reaction temperature. The rate constants for desorption (k_i^{des}) are calculated from the forward rate constants (k_i^{ads}) and the equilibrium constant (K_i), guaranteeing thermodynamic consistency:

$$k_i^{des} = \frac{k_i^{ads}}{K_i} = k_i^{ads} \exp\left(\frac{\Delta G_i(T,p)}{k_B T}\right) \tag{5}$$

Here, ΔG_i is the change in Gibbs free energy upon reaction. The gas-phase entropy contribution to the Gibbs free energy is given by thermodynamic tables for H_2,[41] and calculated from the gas-phase partition functions for the carbon-based molecules.[42−44] The entropy of the adsorbed reactant is calculated within the harmonic approximation.[40] Rate constants for the surface reactions are calculated with harmonic transition state theory as:[45]

$$k_{TST} = \frac{k_B T}{h}\frac{q_0^{\ddagger}}{q} \exp\left(-\frac{\Delta E_a}{k_B T}\right) \tag{6}$$

Here, h is Planck's constant, $q_0^{\ddagger}$ is the partition function of the transition state referenced to the zero energy of the initial state (excluding the reaction coordinate), and q is the partition function of the initial state. The term ΔE_a corresponds to the reaction barrier.

The dependence of the reaction kinetics on the reactant concentration and on the elementary steps is investigated by calculating the reaction orders (n_i) and the apparent activation energy (E_{app}). The reaction orders are calculated as:[40]

$$n_i = p_i \frac{\partial[\ln(r_x)]}{\partial p} \tag{7}$$

Here, p_i is the pressure of the reacting species of interest, and r_x is the net rate of reaction. We have computed the reaction orders of methylcyclohexane (C_7H_{14}), toluene (C_7H_8), and hydrogen (H_2). Calculation of the apparent activation energy enables direct comparison to experimental observations. The apparent activation energy is calculated as:[40]

$$E_{app} = k_b T^2 \frac{\partial \ln(r_x)}{\partial T} \tag{8}$$

The degree of rate control (DRC) explores the sensitivity of the net reaction rate on the elementary steps. The DRC is calculated according to[46]

$$\chi_i = \frac{k_i}{r_x}\left(\frac{\partial r_x}{\partial k_i}\right)_{K_i} \tag{9}$$

Here, k_i is the rate constant of the elementary reaction step i, r_x is the net reaction rate, and K_i is the equilibrium constant of the same elementary step. The derivative is taken with respect to the rate constant while keeping K_i fixed. This is done by numerical differentiation of the rate with respect to the rate constant, while changing the rate constant by 10%. A positive/negative value of χ_i indicates the elementary step is rate-controlling/inhibiting the net rate. The sum of χ_i over all the reaction steps equals unity, whereas a value of one for an individual step indicates the step is rate-determining.[46]

RESULTS

Reaction Thermodynamics

The overall reaction for the conversion between MCH and toluene is:

$$C_7H_{14} \leftrightarrow C_7H_8 + 3H_2 \tag{10}$$

The enthalpy of the dehydrogenation reaction is measured to be $\Delta H^\circ = 2.13$ eV.[14] We calculate the enthalpy of the dehydrogenation reaction to be 1.85 eV. The calculated underestimation is a common issue with the applied exchange-correlation functional describing molecular systems with a C−H backbone.[47−50] The Gibbs free energy change ($\Delta G = \Delta H - T\Delta S$) at hydrogenation and dehydrogenation conditions is shown in Figure 1.

For typical hydrogenation conditions ($p[C_7H_{14}/H_2/C_7H_8]$ = [0.10:20.00:1.00] bar),[17,18] Figure 1 (top) shows that the hydrogenation reaction is exergonic up to 440 K. At this point, the competition in the entropy contribution of the final and initial state gas-phase molecules induces a change in direction of the reaction, making the dehydrogenation reaction preferred. For typical dehydrogenation conditions ($p[C_7H_{14}/H_2/C_7H_8]$

https://doi.org/10.1021/acscatal.6c01477
ACS Catal. 2026, 16, 12123−12134

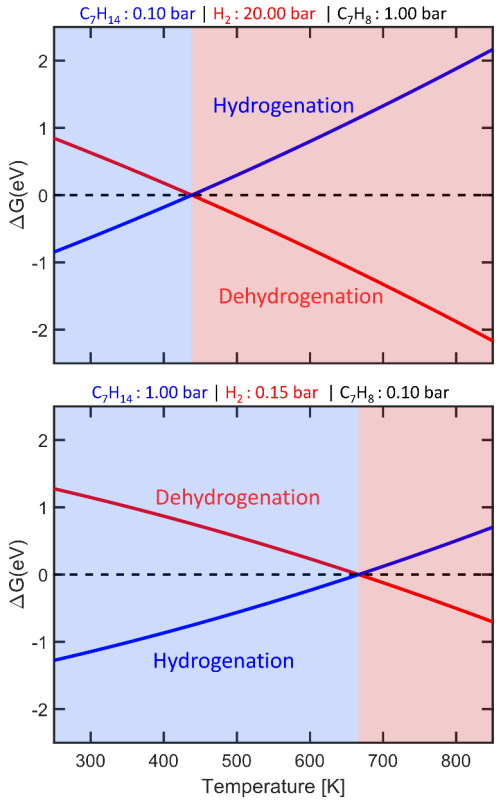

Figure 1. Gibbs free energy change as a function of temperature for MCH/toluene conversion under typical (top) hydrogenation conditions $p[C_7H_{14}/H_2/C_7H_8]$ = [0.10:20.00:1.00] bar and typical (bottom) dehydrogenation conditions $p[C_7H_{14}/H_2/C_7H_8]$ = [1.00:0.15:0.10] bar.

= [1.00:0.15:0.10] bar),[12,13] Figure 1 (bottom), the entropy gain at higher temperatures makes the reaction exergonic at temperatures higher than 665 K. These results highlight the reversibility of the reaction and provide a guide on the relevant temperature regimes for the two reactions. The underestimation of the enthalpy change of the reaction results in a temperature shift with respect to experiments by about 70 K, well within the accuracy of DFT-based kinetic simulations.[47−50]

Catalytic Cycle

We consider a sequential hydrogenation/dehydrogenation mechanism, including the hydrodemethylation of toluene to benzene and methane, Figure 2. Following ref 13 we assume that the conversion reaction proceeds as, $C_7H_{14} \leftrightarrow C_7H_{14}^* \leftrightarrow C_7H_{13}^* \leftrightarrow C_7H_{12}^* \leftrightarrow C_7H_{11}^* \leftrightarrow C_7H_{10}^* \leftrightarrow C_7H_9^* \leftrightarrow C_7H_8^* \leftrightarrow C_7H_8$. Demethylation is considered for toluene and proceeds as $C_7H_8 \leftrightarrow C_7H_8^* \leftrightarrow C_6H_5^* \leftrightarrow C_6H_6^* \rightarrow C_6H_6$. Although the same reaction cycle applies for the two directions of the reaction, the conditions and surface coverages will modify the potential energy diagram depending on the direction.

Adsorption of C_7H_{14} and C_7H_8 on Pt(111)

The MCH to toluene conversion begins and ends with adsorbed C_7H_{14} and C_7H_8. Hence, we pay special attention to these configurations. Figure 3 shows the adsorbed configurations of MCH and toluene on pristine Pt(111) and a Pt(111) surface with 8 pre-adsorbed hydrogen atoms (0.5 ML). The

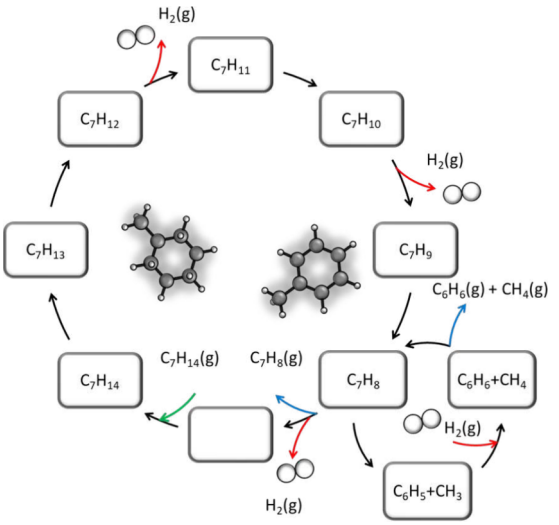

Figure 2. Schematic of the investigated catalytic cycle for MCH/toluene conversion and the competing toluene demethylation over Pt(111). The clockwise direction of the cycle shows dehydrogenation, whereas the counter clockwise direction shows the hydrogenation. The empty box at the bottom of the cycle represents the pristine surface. Hydrogen desorption steps are indicated by red arrows, adsorption of MCH by a green arrow, and desorption of possible products (toluene, benzene, and methane) with blue arrows. A ball and stick model is used to represent the gas-phase molecules, with carbon (grey) and hydrogen (white).

pristine surface corresponds to dehydrogenation conditions, whereas the H-covered surface corresponds to hydrogenation conditions, see the Supporting Information (SI) for a thermodynamic analysis.

MCH and toluene adsorb with different mechanisms on Pt(111). MCH adsorbs through electrostatic and van der Waals interactions, with an adsorption energy of −1.40 eV. MCH has three hydrogen atoms pointing towards Pt atoms with the center of the cyclic ring over an hcp hollow site and the methyl group over a neighboring fcc hollow site (Figure 3a). The average C−Pt distance is 3.26 Å, and the average C−H distance is 1.10 Å. The preferred adsorption configuration is in agreement with a previous study.[22] In the case of toluene (Figure 3b), the molecule is chemisorbed with an energy of −2.48 eV. The average C−Pt distance is 2.18 Å, thus, much shorter than in the case of MCH. Toluene adsorbs with the center of the ring over a bridge site, with the molecule connecting to four surface atoms. The ring makes two π-bonds (with the ipso-carbon taking part in one of these) and two σ bonds with the surface. The methyl group is positioned in a semi-bridge configuration, pointing away from the surface. This adsorption mode is also consistent with a previous report.[22]

The molecules adsorb in a similar way on the surface with a hydrogen coverage of 0.5 ML as on the pristine surface, Figure 3c,d). The adsorption energy of MCH on 8H/Pt(111) is −1.33 eV, which is only slightly lower than on the pristine surface. The similar adsorption energies is reasonable given the mechanisms for adsorption. A larger effect of hydrogen on the surface is calculated for toluene, where the adsorption energy is −1.77 eV. The clear reduction of the adsorption energy is in this case related to the fact that adsorbed H and

https://doi.org/10.1021/acscatal.6c01477
ACS Catal. 2026, 16, 12123−12134

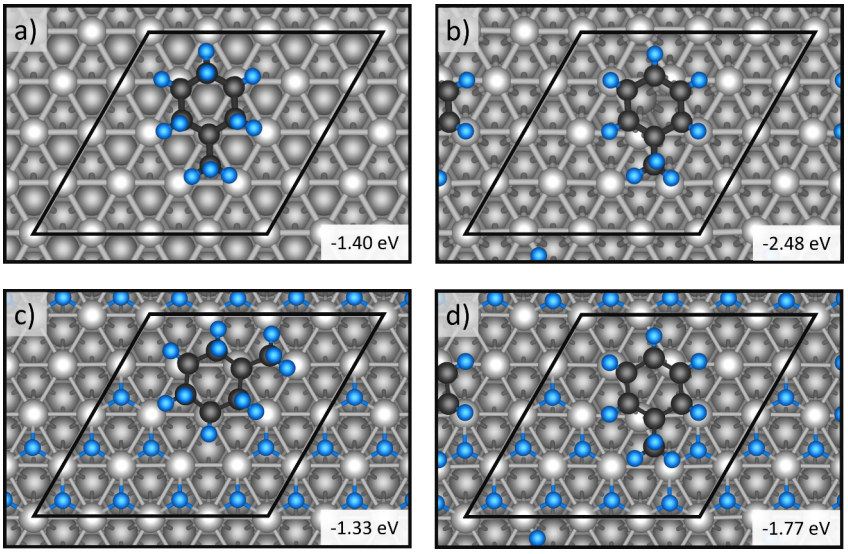

Figure 3. Preferred adsorption configurations of (a) C_7H_{14} on Pt(111), (b) C_7H_8 on Pt(111), (c) C_7H_{14} on H/Pt(111) and (d) C_7H_8 on H/Pt(111). The calculated adsorption energy is shown in the bottom right corner of each structure. Atomic color code: platinum (light grey), carbon (dark grey), hydrogen (blue). The surface cell is indicated with black lines.

toluene are coordinated to the same Pt atoms. The average C−Pt distance is in this case 2.20 Å.

Potential Energy Diagrams

The following three sections describe the potential energy diagrams for MCH dehydrogenation, the unwanted side reaction of toluene hydrodemethylation to benzene, and toluene hydrogenation to MCH.

MCH Dehydrogenation to Toluene and H_2. The zero-point-energy-corrected potential energy diagram for the dehydrogenation of MCH to toluene and molecular hydrogen is presented in Figure 4. The nomenclature used for describing the carbon positions in toluene is shown in Figure S3.

The reaction starts with the adsorption of MCH onto the pristine surface. The first dehydrogenation step is the removal of a hydrogen from the meta-carbon position in the counterclockwise direction from the ipso-carbon site (see Figure S3). The reaction is endothermic by 0.09 eV and has a barrier of 0.77 eV. This is the only endothermic dehydrogenation step along the reaction pathway. The transition state is located with hydrogen going through a semi-atop/semi-bridge site. The distances at the transition state are d[Pt−H] = 1.65 Å, d[Pt−H] = 2.22 Å, and d[C−H] = 1.47 Å. Hydrogen occupies a neighboring hollow fcc site, and the bond scission leads to C_7H_{13}* + H*. All subsequent dehydrogenation steps proceed through transition states with structural configurations similar to those of the first dehydrogenation step (all structures are provided in the SI). The dehydrogenation process leads to the formation of a Pt−C bond of 2.14 Å between the meta-carbon site and the Pt-surface. The substantial shortening of the Pt−C bond compared to MCH leads to a angle between the molecular and surface planes. The C−C distances in the cyclic ring are moderately affected by the dehydrogenation; the average nearest neighbor distance is contracted by 0.01 Å. For the sake of completeness, we also explored the possibility of dehydrogenation from the ipso position. The dehydrogenation from the ipso-carbon site is endothermic by 0.25 eV with respect to adsorbed MCH, making ipso-carbon dehydrogenation less likely to occur than the meta-carbon dehydrogenation.

The reaction diagram proceeds by the desorption of hydrogen to the gas phase as 1/2 H_2. The step is assumed after every dehydrogenation step. The desorption of hydrogen is endothermic by 0.13 eV. The second dehydrogenation step, C_7H_{13}* → C_7H_{12}* + H*, is exothermic by −0.13 eV and has an activation energy of 0.76 eV. The dehydrogenation proceeds in this case from the ipso-carbon position. The transition state is similar to the one described for the first step. In the final state, hydrogen occupies the nearest fcc hollow site to the ipso-carbon. The Pt−C(ipso) distance decreases from 3.09 Å in C_7H_{13}* to 2.15 Å after dehydrogenation. The desorption of hydrogen is in this case endothermic by 0.33 eV. The third dehydrogenation step proceeds from a meta-position, leading to C_7H_{11}* + H*, which is exothermic by −0.37 eV. The reaction barrier is lower than the two previous steps, being 0.47 eV. The transition state is located directly over the Pt atom, at which the meta-carbon is located before the dehydrogenation. In the final state, C_7H_{11} has a planar configuration on the surface with the two meta-carbons and the ipso-carbon bound atop the surface atoms and hydrogen located at the adjacent hcp hollow site. The difference in adsorption energy of hydrogen in the fcc and hcp hollow sites on the pristine Pt(111) is only 0.06 eV, with the fcc being preferred. The change in adsorption site for hydrogen is caused by lateral repulsion of the adsorbates. The subsequent desorption of hydrogen is endothermic by 0.32 eV. The fourth dehydrogenation step proceeds from the ortho-carbon in the clockwise direction with respect to the ipso-carbon and is exothermic by −0.31 eV. The reaction has an activation energy of 0.66 eV. By symmetry, the dehydrogenation from the ortho carbon is iso-stable. The desorption of the hydrogen is endothermic by 0.28 eV. The fifth dehydrogenation proceeds from the second ortho-carbon site and is exothermic by ΔE = −0.22 eV. The barrier is in this case 0.71 eV. The dehydrogenation occurs on the atop site, and hydrogen occupies an hcp hollow site in the final state. The desorption of hydrogen is endothermic by 0.29 eV. The last dehydrogenation step, with

https://doi.org/10.1021/acscatal.6c01477
ACS Catal. 2026, 16, 12123−12134

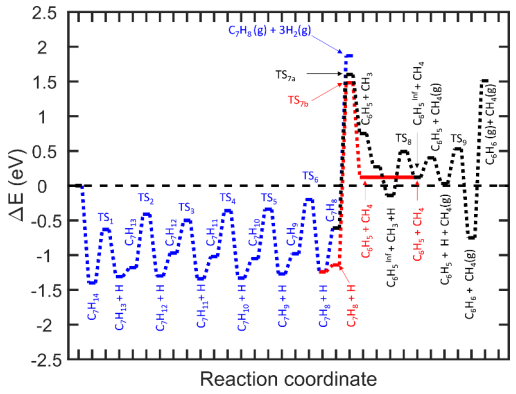

Figure 4. Zero-point energy corrected potential energy diagram of methylcyclohexane dehydrogenation to toluene and hydrogen (blue). Hydrodelakylation under direct demethylation (black) and hydrogenolysis (red) of toluene are also explored.

the hydrogen coming from the para-carbon position, results in toluene and hydrogen on the surface. The reaction is exothermic by −0.20 eV and has the largest barrier in the dehydrogenation process, being 0.78 eV. The transition state is over the atop configuration, and hydrogen occupies an fcc hollow site in the final state. The last hydrogen desorption step is endothermic by 0.56 eV. Finally, the desorption energy of toluene to the gas-phase is endothermic by 2.48 eV, which is the highest barrier in the reaction diagram.

To summarize, the dehydrogenation of MCH proceeds via C−H scissions from meta → ipso → meta → ortho → ortho → para. However, there are probably possibilities of alternative dehydrogenation orders with similar energetics. For example, an adsorption configuration of C_7H_{14} where the hydrogen on the ipso-carbon points away from the surface is energetically competitive (see SI section "Alternative MCH Dehydrogenation Order"). The dehydrogenation of this alternative initial adsorption configuration leads to a situation where the last hydrogen in the dehydrogenation mechanism ($C_7H_9^* \rightarrow C_7H_8^* + H^*$) points away from the surface, blocking the last dehydrogenation step. In such a case, hydrogen diffusion (ipso → ortho) in the cyclic ring is possible with a reaction barrier of around 1.6 eV, allowing for the last dehydrogenation step to occur. It is, in principle, possible that the reaction steps proceed via metastable adsorption configurations. However, we do not expect such effects to affect conclusions owing to the similarity between all evaluated hydrogenation barriers and transition state structures (Figure S6).

Toluene Hydrodemethylation to Benzene. The hydrodemethylation of toluene to benzene and methane ($C_7H_8 + H_2 \rightarrow C_6H_6 + CH_4$) is of particular interest for catalytic looping of MCH/toluene. Hydrodemethylation is detrimental to the overall use of MCH/toluene as LOHC as it (i) contaminates the H_2 product feed, which potentially forces more stringent aftertreatment of the produced hydrogen, and (ii) destroys the carrier molecule and consumes hydrogen, reducing the volumetric and gravimetric capacity of hydrogen storage over time. Here, we investigate the possibility of toluene hydrodemethylation to benzene and methane through two scenarios: (i) $C_7H_8^* \rightarrow C_6H_5^* + CH_3^*$ (direct demethylation of toluene), and (ii) $C_7H_8^* + H^* \rightarrow C_6H_5^* + CH_4^*$ (hydrogenolysis of toluene). The calculated relative energies for the explored scenarios are presented in Figure 4. Hydrodemethylation of other reaction intermediates than toluene is, in principle, possible. However, given that the reaction barriers for the dehydrogenation reactions are considerably smaller than the barrier for C−C scission, this suggests that hydrodemethylation is most probable for the carbon species with the highest adsorption energy, which is toluene.

Exploring first (i) direct demethylation of toluene (black curve), the reaction proceeds from adsorbed toluene. The process has a barrier of 2.21 eV, and is endothermic by 1.65 eV. The C−C breaking occurs atop the Pt-atom over which the methyl group is positioned. The methyl and phenyl groups are in the final state bound to the same Pt-atom, which protrudes from the surface by 0.73 Å. The calculated barrier and reaction energy are in agreement with a previous reports using the same level of theory.[S1] The next step in the potential energy diagram reported in Figure 4 is to separate the methyl and phenyl groups to infinite distances, which is connected with stabilization. The reaction continues with the independent hydrogenation of methyl and phenyl. Adsorbing hydrogen from the gas-phase is exothermic by −0.52 eV. The formation of physisorbed methane has a barrier of 0.63 eV, and the reaction is endothermic by 0.09 eV. The reaction continues with desorption of CH_4 and another hydrogen adsorption step. The barrier for benzene formation is 0.50 eV, and the reaction is exothermic by −1.01 eV. Finally, desorption of benzene is associated with an energy of 2.26 eV. The gas-phase state of benzene and methane less endothermic than the final state for toluene and $3H_2$ by −0.36 eV.

Exploring the (ii) hydrogenolysis of toluene (red curve), the reaction starts by diffusion of the adsorbed hydrogen to a position close to the methyl group. From this state, the hydrogenolysis proceeds with a barrier of 2.46 eV. The barrier is higher for hydrogenolysis than for direct demethylation, and the final state of the reaction is chemisorbed phenyl and physisorbed methane. The reaction proceeds from this step in the same way as in the first scenario.

Toluene Hydrogenation to Methylcyclohexane. Toluene hydrogenation to MCH is reversed with respect to MCH dehydrogenation to toluene. However, as the reaction conditions are different for the two reactions, the surface coverages are different. A thermodynamic analysis (see Figure S1) shows that the dehydrogenation reaction ($T > 673$ K; $p[H_2] \sim 0.2$ bar) occurs on a low-coverage surface, whereas the hydrogenation reaction ($T < 523$ K; $p[H_2] \sim 20.0$ bar) occurs over a surface with a hydrogen coverage of ∼0.75 ML. The configurational possibilities with a high hydrogen coverage make a complete DFT-sampling of the configurations infeasible. We have here adopted a pragmatic view of the configurational problem. The potential energy diagram for toluene hydrogenation on the hydrogen-covered Pt(111) is constructed from the adsorption energies of toluene and MCH on a surface with 0.5 ML coverage of hydrogen. The reaction barriers are slightly increased with respect to the pristine surface to account for the repulsive interactions caused by the hydrogen atoms. The increase in barrier is evaluated explicitly for the first hydrogenation step ($C_7H_8^* + H^* \rightarrow C_7H_9^* + *$) on a surface covered with 1 ML of hydrogen. The choice of studying the hydrogenation step on the fully covered surface is to provide an upper bound of the barrier. The barrier for toluene hydrogenation to MCH on the fully H-covered surface is 0.94 eV, which is slightly higher than on the pristine (0.78 eV). Given

https://doi.org/10.1021/acscatal.6c01477
ACS Catal. 2026, 16, 12123−12134

the similarity of the barrier and the structure of the transition state, all barriers are increased by 0.2 eV. The adjusted potential energy for the full hydrogenation reaction is presented in Figure S5 and the kinetic parameters used in the simulations are shown in Table S1. Importantly, the analysis below shows that the reaction kinetics are insensitive to the hydrogenation barriers.

Kinetic Simulations

A mean-field microkinetic model is constructed from the DFT calculated values (Figure 4) to investigate the kinetic behavior of the proposed catalytic cycle (Figure 2). The considered elementary steps and the kinetic parameters (forward and backwards activation energies and pre-exponential factors calculated at 673 K) are shown in Table 1.

Kinetics of MCH Dehydrogenation. MCH dehydrogenation simulations are performed at typical reaction conditions, i.e., $T = 573-923$ K and $p[C_7H_{14}] = 1.00$ bar. The simulations have been done with 5% conversion to toluene and hydrogen, whereas hydrodemethylation conversion was considered at 1% with respect to MCH. The results are not sensitive to the choices of conversion; however, some conversion is needed not to unrealistically favor the entropic gain in the forward reaction. Re-adsorption of benzene and methane is not considered in the model. Adsorbed cyclic carbon molecules occupy four Pt sites; thus, their combined total surface coverage is constrained to a maximum of 0.11 ML. The saturation coverage for the cyclic carbon molecules is in line with experimental observations.[37,39] The kinetic results are presented as a function of temperature in Figure 5. The shaded parts in Figure 5a,b are included just for reference, as they correspond to temperatures where the thermodynamics of the reaction favor hydrogenation.

The turnover frequency for MCH dehydrogenation (Figure 5a) becomes positive at 661 K and peaks at 705 K. Hydrodemethylation of toluene is positive in the entire temperature regime and reaches a maximum at $T = 779$ K. The TOF of toluene hydrodemethylation is at most two orders of magnitude smaller than the TOF of MCH dehydrogenation (Figure 5f). As the two reactions peak at different temperatures, it would be possible to suppress hydrodemethylation even further by operating the reaction close to the maximum for MCH dehydrogenation. The change in sign of the TOF for MCH dehydrogenation correlates with a decrease in toluene coverage and a simultaneous increase in the number of free sites. The surface is above 661 K covered by H and small amounts of toluene and benzene (Figure 5b). The H coverage is 0.66 ML at 661 K and drops to 0.08 ML at 923 K. The coverages of toluene and benzene peak at 655 and 723 K, respectively reaching a maximum value of 0.03 ML and 0.01 ML, respectively.

The dependence of the TOF for MCH dehydrogenation on the elementary reactions steps is evaluated by a degree of rate control analysis (DRC), Figure 5c. From the DRC-analysis, we find that the MCH dehydrogenation TOF is controlled by the second dehydrogenation step ($C_7H_{13}^* \rightarrow C_7H_{12}^* + H^*$) and to some extent by the first ($C_7H_{14}^* \rightarrow C_7H_{13}^* + H^*$).

The DRC of the second dehydrogenation step is 0.95 at 670 K and drops to 0.85 at 810 K. Simultaneously, the first dehydrogenation step increases from 0.03 at 670 K to 0.12 at 810 K. The finding that the first and second hydrogenation steps control the reaction agrees with experimental observations for Pt/Al_2O_3 catalysts, where the rate-determining step has been suggested to be located somewhere between MCH adsorption and the dehydrogenation to methylcyclohexene (C_7H_{12}).[13,52]

The reaction orders (n_i), Figure 5d, are calculated with a differential increase in pressure of 12%. The reaction order of MCH is close to unity in the entire temperature range, whereas the reaction orders of H and toluene are close to zero. Experimentally, the reaction orders have been measured to be $n_{C_7H_{14}} = 1$, at relatively low pressures of MCH ($p[C_7H_{14}] < (0.5$ bar$]$),[12] whereas the reaction orders of hydrogen and toluene are slightly negative[15] or zero.[13] The reaction order close to unity for MCH implies that stabilization of MCH on the surface is one potential way of increasing the dehydrogenation rate. The MCH reaction order has been measured to decrease to zero with higher pressure, $p[C_7H_{14}] > (1.5$ bar) for MCH dehydrogenation over supported Pt nanoparticles. We do not find this change in our model; however, stabilization of MCH adsorption reduces the reaction order to near-zero (Figure S11). We speculate that the reason the model does not capture the change in reaction order of MCH is related to the use of Pt(111) as the model catalyst.

Table 1. Elementary Steps in the Reaction Network and Calculated Kinetic Parameters: Elementary Steps and Zero Point-Energy Corrected Forward (E_f) and Backward (E_b) Barriers together with Pre-Exponential Factors[a,b]

no.	reaction	E_f (eV)	E_b (eV)	A_f	A_b
R_1	$H_2(g) + 2^* \leftrightarrow 2H^*$	0.00	1.00	3.02×10^3	2.95×10^7
R_2	$C_7H_{14}(g) + ^* \leftrightarrow C_7H_{14}^*$	0.00	1.40	4.31×10^2	2.30×10^{11}
R_3	$C_7H_{14}^* + ^* \leftrightarrow C_7H_{13}^* + H^*$	0.77	0.64	9.52×10^{11}	1.32×10^{13}
R_4	$C_7H_{13}^* + ^* \leftrightarrow C_7H_{12}^* + H^*$	0.76	0.82	7.42×10^{12}	2.13×10^{13}
R_5	$C_7H_{12}^* + ^* \leftrightarrow C_7H_{11}^* + H^*$	0.47	0.78	9.80×10^{12}	2.00×10^{13}
R_6	$C_7H_{11}^* + ^* \leftrightarrow C_7H_{10}^* + H^*$	0.66	0.86	3.25×10^{13}	9.64×10^{12}
R_7	$C_7H_{10}^* + ^* \leftrightarrow C_7H_9^* + H^*$	0.71	0.81	5.98×10^{13}	3.65×10^{13}
R_8	$C_7H_9^* + ^* \leftrightarrow C_7H_8^* + H^*$	0.78	1.00	4.52×10^{13}	1.41×10^{13}
R_9	$C_7H_8^* \leftrightarrow C_7H_8(g) + ^*$	2.48	0.00	1.18×10^7	4.45×10^2
R_{10}	$C_7H_8^* + ^* \leftrightarrow C_6H_5^* + CH_3^*$	2.21	1.65	2.21×10^{14}	1.31×10^{13}
R_{11}	$C_6H_5^* + H^* \leftrightarrow C_6H_6^* + ^*$	0.50	1.23	1.11×10^{13}	3.24×10^{13}
R_{12}	$C_6H_6^* \rightarrow C_6H_6(g) + ^*$	2.32		2.10×10^{14}	
R_{13}	$CH_3^* + H^* \rightarrow CH_4(g) + 2^*$	0.86		3.58×10^{13}	

[a]Pre-exponential factors are calculated at 673 K and are denoted A_f and A_b for forward and backward reactions, respectively. The pre-exponential factors of surface reactions are reported in (s^{-1}), whereas adsorption steps are reported in (Pa^{-1} s^{-1}). [b]The kinetic parameters are calculated for a pristine surface.

https://doi.org/10.1021/acscatal.6c01477
ACS Catal. 2026, 16, 12123−12134

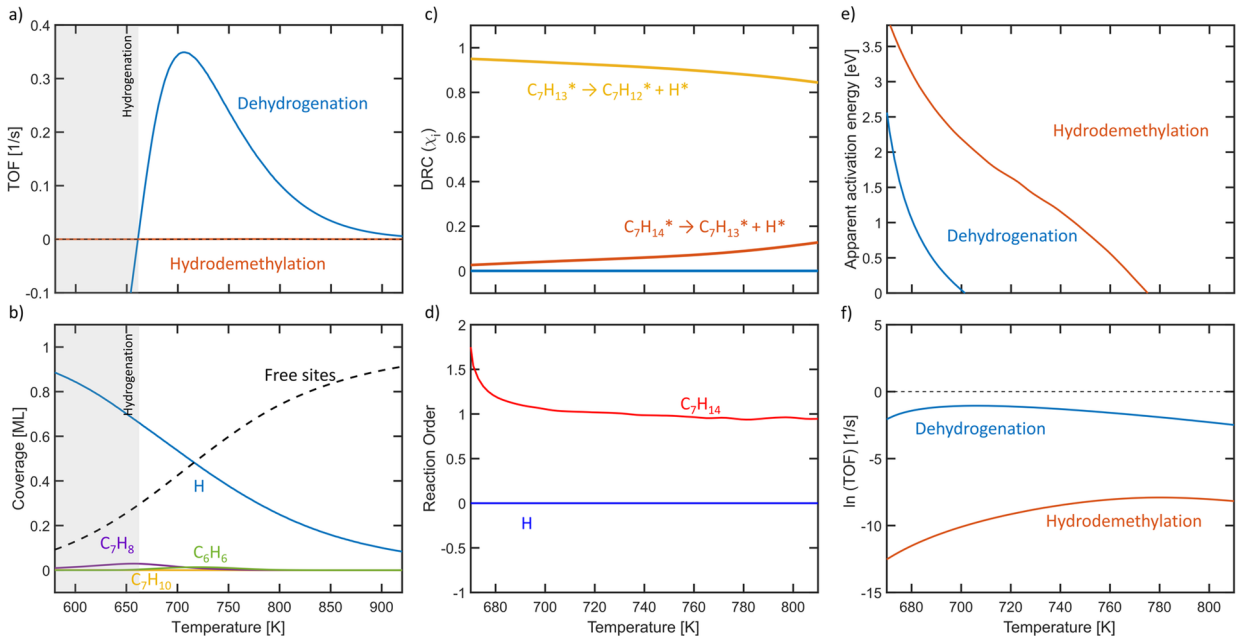

Figure 5. Temperature-dependent kinetic analysis of MCH dehydrogenation reaction: (a) surface coverage, (b) turnover frequency, (c) degree of rate control, (d) reaction orders, (e) apparent activation energy, and (f) logarithm of turnover frequency. The simulations are performed at T = 573−923 K and $p[C_7H_14]$= 1.00 bar, considering 5% conversion to C_7H_8 and H_2 and 1% for toluene hydrodemethylation.

The degree of rate control and reaction orders for toluene hydrodemethylation are shown in Figure S9. The DRC analysis for hydrodemethylation shows zero values for all reaction steps except desorption of benzene and demethylation of toluene, which is a competing reaction path. The reaction orders are zero for all reactants, which is in line with the DRC analysis, as benzene desorption controls the reaction at typical dehydrogenation conditions.

The calculated apparent activation energy for dehydrogenation of MCH and the hydrodemethylation of toluene as a function of temperature is shown in Figure 5e. The apparent activation for MCH dehydrogenation decreases with temperature, from 2.3 eV at 670 K to zero at 702 K, where the TOF has its maximum. Experimentally, the apparent activation energy has been reported to be between 0.77 and 0.39 eV, depending on particle size,[16] comparable to our calculated values near T = 685−690 K. With increasing temperature, the apparent activation energy changes sign, as the TOF has a maximum. The apparent activation energy for hydrodemethylation of toluene is higher than that of MCH dehydrogenation. At 670 K, the apparent activation energy for hydrodemethylation of toluene is 3.9 eV and decreases with increasing temperature, until it reaches a value of zero at 775 K. The high apparent activation energy for hydrodemethylation in the model makes this process not competitive with the dehydrogenation of MCH. The fact that hydrodemethylation is observed experimentally suggests that this reaction occurs on undercoordinated sites where breaking of C−C bonds generally is believed to have a lower activation energy.

Kinetics of Toluene Hydrogenation. Toluene hydrogenation simulations are performed at T = 273−623 K and $p[C_7H_8]$ = 1.0 bar and $p[H_2]$ = 20 bar, considering 10% conversion of toluene, whereas hydrodemethylation conversion was considered at 1% with respect to MCH. The results of the simulations are presented as a function of temperature in Figure 6.

The calculated turnover frequency for toluene hydrogenation lights off at about 425 K (Figure 6a). The rate increases with temperature and reaches a maximum value at T = 527 K. The rate drops after this temperature and becomes negative at temperatures higher than 580 K. This is the temperature where the reversed reaction is thermodynamically preferred. The TOF is about two orders of magnitude lower than for the dehydrogenation reaction. The lower TOF is related to the higher barriers for the hydrogenation than for the dehydrogenation reactions as a result of the high hydrogen coverage. The TOF for the hydrodemethylation of toluene is negligible in the entire temperature range. The TOF for hydrodemethylation is at its maximum, about 5 orders of magnitude lower than that of the hydrogenation reaction. The logarithm of the turnover frequency for both reactions is presented in Figure 6f to highlight the differences between the two TOFs.

The surface is mainly covered by hydrogen over the entire temperature range (Figure 6a). The coverage of H drops from 1 ML at 273 K to 0.69 ML at 623 K. The coverages of the cyclic carbon molecules are all close to zero. Toluene has a maximum coverage of 0.01 ML at 543 K.

From the DRC analysis, Figure 6c, we find that the reaction kinetics is determined by three elementary steps. The initial hydrogenation of toluene (C_7H_8* + H* → C_7H_9*) is controlling the hydrogenation in the lower temperature regime (T < 410 K), whereas the hydrogenation of methylcyclohexene (C_7H_{12}* + H* → C_7H_{13}*) controls the reaction at higher temperatures (T > 410 K). At intermediate temperatures, the hydrogenation of methylcyclohexadiene (C_7H_{10}* + H* → C_7H_{11}*) plays a moderate role in the reaction. The DRC analysis of the hydrogenation reaction correlates with the results for the dehydrogenation reaction in the sense that the hydrogenation of methylcyclohexene (C_7H_{12}) has rate control.

We find the reaction orders in H_2 and C_7H_8 to be zero for the entire temperature interval. This result is an effect of the

https://doi.org/10.1021/acscatal.6c01477
ACS Catal. 2026, 16, 12123−12134

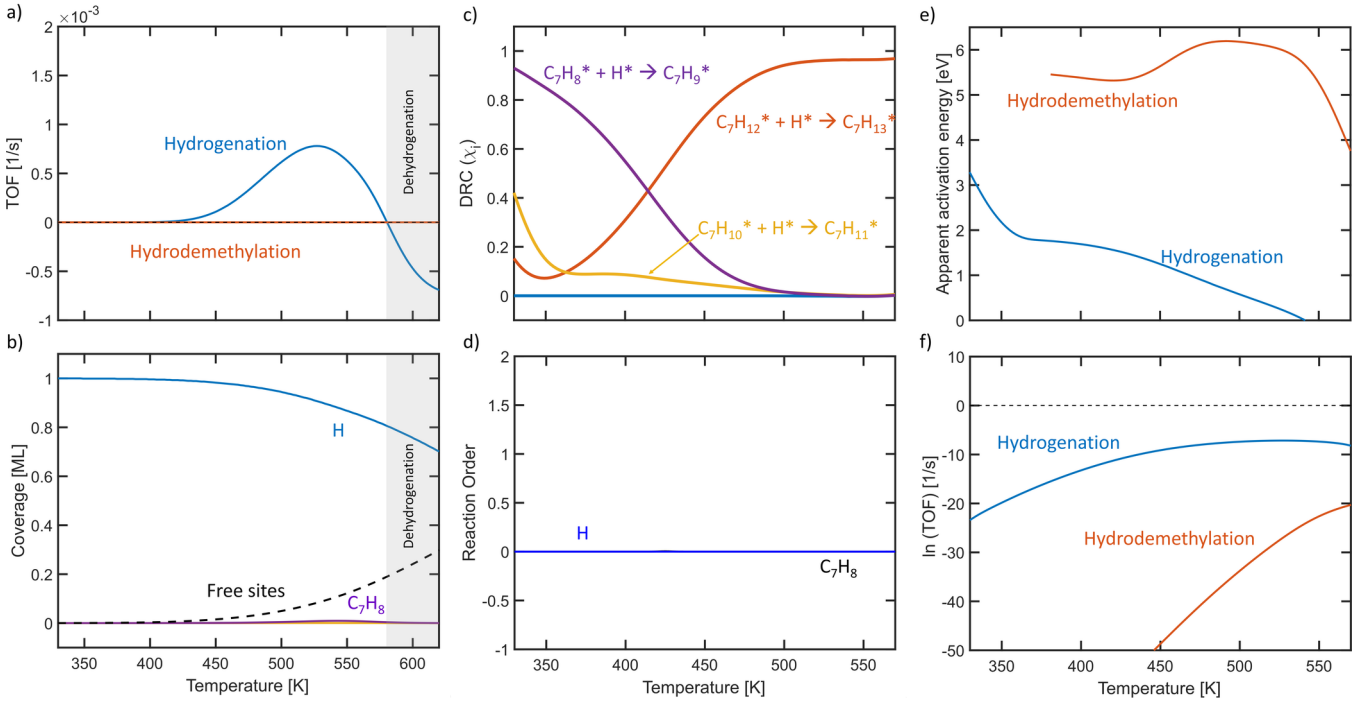

Figure 6. Temperature-dependent kinetic analysis of toluene hydrogenation reaction: (a) surface coverage, (b) turnover frequency, (c) degree of rate control, (d) reaction orders, (e) apparent activation energy, (f) logarithm of turnover frequency. The simulations are performed at $T = 273-623$ K and $p[C_7H_8] = 1.0$ bar and $p[H_2] = 20.0$ bar and 10% conversion.

high hydrogen coverage. Experimentally, the reaction orders for toluene hydrogenation have been measured to be between 1.0−1.2 and 0.1−0.7 for H_2 and toluene, respectively, at a total pressure of 1 bar at Pt NP of 2.5 nm.[18,20] The experiments indicate that the coverage of H is low at the experimental conditions (∼0.8% toluene and ∼10% H_2 at a temperature of 473 K).

The calculated apparent activation energy for hydrogenation of toluene to MCH and for the hydrodemethylation of toluene to benzene as a function of temperature is reported in Figure 6e. We find that the apparent activation for toluene hydrogenation decreases with temperature, from 3.2 eV at 330 K to a value of zero at 540 K. The apparent activation energy for toluene hydrogenation on nickel has been estimated to be about 0.37 eV in a temperature range between 400 and 460 K.[53] The apparent activation energy of toluene hydrodemethylation to benzene is calculated to be ∼5 eV from 380 K onward, showing relatively small changes at temperatures below 523 K, which is consistent with the low rate of the reaction.

■ DISCUSSION

The results obtained for the dehydrogenation of MCH agree with experimental observations.[11,12,14] The TOF is controlled by the first two dehydrogenation steps and toluene desorption. Moreover, the reaction is first-order with respect to C_7H_{14}. The analysis suggests that the TOF can be increased by reducing the barriers for the first dehydrogenation steps and/or changing the stability of MCH and toluene on the surface.

To test these hypotheses, we separately lowered the barrier for the first hydrogenation step and the desorption energy of toluene, whereas the desorption energy of MCH was increased (Figure 7). Note that the stabilization of only one intermediate with respect to the gas-phase changes the equilibrium of the reaction. We find that the changes in all cases increase the TOF. Reducing the barrier for MCH dehydrogenation increases the rate by about a factor of 5. A similar change is obtained by stabilizing MCH on the surface. Reducing the barrier for toluene desorption has a positive but minor effect (+9%) on the TOF for MCH dehydrogenation.

The low TOF for the unwanted toluene hydrodemethylation (Figure 5) suggests that this side reaction experimentally occurs on more reactive sites than Pt(111). Undercoordinated sites, like steps and kinks, are known to facilitate C−C bond breaking with respect to Pt(111). This effect has been experimentally observed for the dehydrogenation of MCH[12] and has also been computationally investigated using a similar level of theory as here.[51] Manabe et al. reported a reduction in the activation energy by 0.61 eV for the demethylation of toluene on Pt(311) as compared to Pt(111).[51] We examined the effect of steps on the hydrodemethylation rate by simply using the activation energy reported by Manabe et al. ($E_a[C_7H_8 \rightarrow C_6H_5 + CH_3] = 1.61$ eV) in the microkinetic model. Using this simple approach, we find that inclusion of undercoordinated sites increases the hydrodemethylation TOF by more than one order of magnitude with respect to the reaction occurring on Pt(111) (Figure S10). The TOF for hydrodemethylation depends largely on the stability of toluene on the surface. A moderate destabilization of toluene on the surface reduces the TOF for hydrodemethylation significantly while simultaneously improving the TOF for MCH dehydrogenation (Figure S10). This finding potentially provides some rationalization for the use of additives on Pt-based catalysts to hinder toluene hydrodemethylation.[19]

Turning to the toluene hydrogenation, the analysis in Figure 6 shows that the reaction is controlled by the

https://doi.org/10.1021/acscatal.6c01477
ACS Catal. 2026, 16, 12123−12134

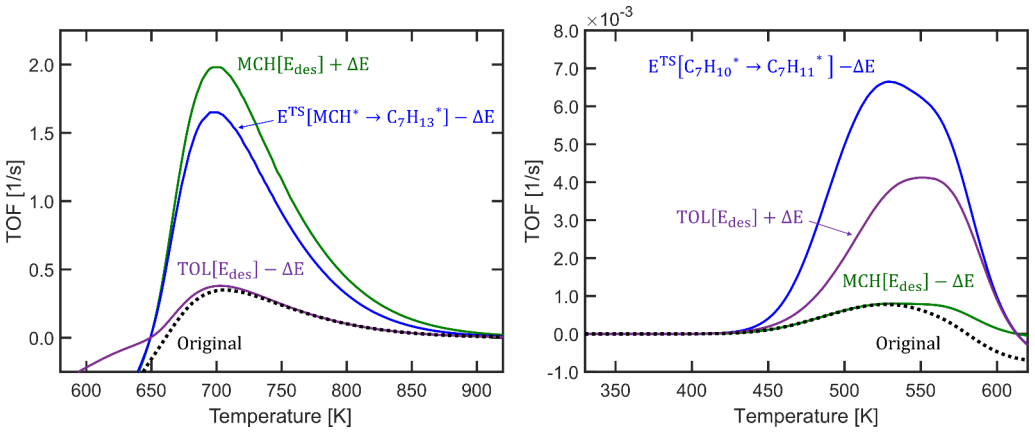

Figure 7. Change in the turnover frequency upon the stabilization/destabilization of selected intermediates by $\Delta E = 0.1$ eV. (Left) MCH dehydrogenation and (right) toluene (TOL) hydrogenation. The simulations are performed using same reaction conditions as in Figure 5 (left) and Figure 6 (right).

hydrogenation barriers. We explored the effect on the TOF by modestly lowering these barriers, of which the most significant case is shown in Figure 7. Lowering the barrier for C_7H_{10} hydrogenation improves the TOF by about one order of magnitude. Separately reducing any of the hydrogenation barriers has a similar positive effect on the TOF. In addition to the hydrogenation barriers, stabilizing toluene on the surface increases the TOF by about 5 times. Destabilizing MCH on the surface has a marginal effect (+3%) on the TOF.

■ CONCLUSIONS

Liquid organic hydrogen carriers (LOHC) are a technology to store hydrogen at standard conditions. The technology is based on efficient catalysts for the hydrogenation and dehydrogenation of a carrier molecule. Here, we have used density functional theory calculations and mean-field microkinetic modeling to investigate the conversion between methylcyclohexane and toluene $[C_7H_{14} \leftrightarrow C_7H_8 + 3H_2]$ on Pt(111) as a function of temperature, interrogating both hydrogenation and dehydrogenation. In both cases, we have explored the direct conversion route and the competing toluene hydrodemethylation reaction $[C_7H_8 + H_2 \leftrightarrow C_6H_6 + CH_4]$.

For MCH dehydrogenation at typical reaction conditions, we find that the computed temperature dependence on the TOF, reaction orders, and apparent activation energy agrees with experimental observations. The reaction is predicted to light off at temperatures higher than $T = 661$ K, in agreement with the thermodynamics of the gas-phase reaction, reaching a maximum at 705 K. Conversion of MCH to toluene is first order in MCH pressure and controlled by the first two dehydrogenation steps and MCH desorption. Unwanted toluene hydrodemethylation to benzene occurs in the same temperature range as MCH dehydrogenation, reaching a maximum rate at 779 K. The side reaction is controlled by the activation energy for toluene demethylation and the desorption of benzene. The TOF for hydrodemethylation is calculated to be three orders of magnitude lower than that of MCH dehydrogenation, which suggests that uncoordinated sites dominate this reaction in experiments where the TOF for the unwanted reaction is higher.

For the hydrogenation of toluene to MCH at typical reaction conditions, we also find that the predicted temperature dependence on the TOF and apparent activation energy agrees with experimental observations. The reaction is predicted to light off at around 425 K, reaching a maximum at 527 K. Conversion of toluene to MCH is controlled by the first and late hydrogenation steps and the desorption of toluene.

The present work provides a fundamental understanding of (de)hydrogenation of the MCH/toluene pair on Pt surfaces and presents paths for rational design of improved catalysts. The simulations reveal that stabilization of methylcyclohexane adsorption is one potential way to improve the dehydrogenation reaction rate, whereas destabilization of toluene adsorption is predicted to increase the rate of MCH dehydrogenation. Thus, surface modifications that change the adsorption energies are under-explored thermodynamic handles to improve the rates of the reactions.

For the dehydrogenation, surface modifications that stabilize the adsorption of MCH and reduce the first hydrogenation step are predicted to be effective ways to improve the reaction rate. For the hydrogenation of toluene, decreasing the barriers for the elementary hydrogenation steps increases the TOF. The TOF for the competing hydrodemethylation reaction is found to be several orders of magnitude lower than the preferred reactions on Pt(111). This suggests that nanoparticles with large Pt(111) facets are preferred to suppress unwanted hydrodemethylation reactions.

■ ASSOCIATED CONTENT

Supporting Information

The Supporting Information is available free of charge at https://pubs.acs.org/doi/10.1021/acscatal.6c01477.

Thermodynamic analysis of surface conditions, alternative methylcyclohexane dehydrogenation order, kinetic analysis of stabilized MCH, kinetic analysis of toluene hydrodemethylation, and kinetic analysis on the potential role of steps (PDF)

Coordinate files for structural models (ZIP)

■ AUTHOR INFORMATION

Corresponding Authors

Alvaro Posada-Borbón – *Department of Physics and Competence Centre for Catalysis, Chalmers University of*

https://doi.org/10.1021/acscatal.6c01477
ACS Catal. 2026, 16, 12123−12134

Technology SE-412 96 Göteborg, Sweden; Email: palvaro@chalmers.se

Henrik Grönbeck – *Department of Physics and Competence Centre for Catalysis, Chalmers University of Technology SE-412 96 Göteborg, Sweden;* Email: ghj@chalmers.se

Author

Tobias Möslinger – *Department of Physics and Competence Centre for Catalysis, Chalmers University of Technology SE-412 96 Göteborg, Sweden*

Complete contact information is available at: https://pubs.acs.org/doi/10.1021/acscatal.6c01477

Notes

The authors declare no competing financial interest.

■ ACKNOWLEDGEMENTS

Financial support is acknowledged from the Wallenberg Initiative Material Science for Sustainability (WISE-AP01-PD02) and the Swedish Research Council (2024-05250). The calculations were performed at NSC via a NAISS grant (NAISS 2024/3-26). The Competence Centre for Catalysis (KCK) is hosted by Chalmers University of Technology and is financially supported by the Swedish Energy Agency and the member companies Johnson Matthey, Perstorp, Powercell, Preem, Scania CV, Umicore, and Volvo Group.

■ REFERENCES

(1) Okada, Y.; Sasaki, E.; Watanabe, E.; Hyodo, S.; Nishijima, H. Development of dehydrogenation catalyst for hydrogen generation in organic chemical hydride method. *Int. J. Hydrogen Energy* **2006**, *31*, 1348–1356.

(2) Teichmann, D.; Arlt, W.; Wasserscheid, P.; Freymann, R. A future energy supply based on liquid organic hydrogen carriers (LOHC). *Energy Environ. Sci.* **2011**, *4*, 2767–2773.

(3) He, T.; Pei, Q.; Chen, P. Liquid organic hydrogen carriers. *J. Energy Chem.* **2015**, *24*, 587–594.

(4) Modisha, P. M.; Ouma, C. N. M.; Garidzirai, R.; Wasserscheid, P.; Bessarabov, D. The prospect of hydrogen storage using liquid organic hydrogen carriers. *Energy Fuels* **2019**, *33*, 2778–2796.

(5) Niermann, M.; Beckendorff, A.; Kaltschmitt, M.; Bonhoff, K. Liquid organic hydrogen carrier (LOHC) – Assessment based on chemical and economic properties. *Int. J. Hydrogen Energy* **2019**, *44*, 6631–6654.

(6) Sekine, Y.; Higo, T. Recent trends on the dehydrogenation catalysis of liquid organic hydrogen carrier (LOHC): A review. *Top. Catal.* **2021**, *64*, 470–480.

(7) Allendorf, M. D.; Stavila, V.; Snider, J. L.; Witman, M.; Bowden, M. E.; Brooks, K.; Tran, B. L.; Autrey, T. Challenges to developing materials for the transport and storage of hydrogen. *Nat. Chem.* **2022**, *14*, 1214–1223.

(8) Niermann, M.; Timmerberg, S.; Drünert, S.; Kaltschmitt, M. Liquid organic hydrogen carriers and alternatives for international transport of renewable hydrogen. *Renewable Sustainable Energy Rev.* **2021**, *135*, No. 110171.

(9) Preuster, P.; Papp, C.; Wasserscheid, P. Liquid organic hydrogen carriers (LOHCs): Toward a hydrogen-free hydrogen economy. *Acc. Chem. Res.* **2017**, *50*, 74–85.

(10) Gianotti, E.; Taillades-Jacquin, M.; Rozière, J.; Jones, D. J. High-purity hydrogen generation via dehydrogenation of organic carriers: A review on the catalytic process. *ACS Catal.* **2018**, *8*, 4660–4680.

(11) Sinfelt, J. H.; Hurwitz, H.; Shulman, R. A. Kinetcs of methylcyclohexane dehydrogenation over Pt–Al_2O_3. *J. Phys. Chem.* **1960**, *64*, 1559–1562.

(12) Van Trimpont, P. A.; Marin, G. B.; Froment, G. F. Kinetics of methylcyclohexane dehydrogenation on sulfided commercial platinum/alumina and platinum-rhenium/alumina catalysts. *Ind. Eng. Chem. Fundam.* **1986**, *25*, 544–553.

(13) Alhumaidan, F.; Cresswell, D.; Garforth, A. Kinetic model of the dehydrogenation of methylcyclohexane over monometallic and bimetallic Pt catalysts. *Ind. Eng. Chem. Res.* **2011**, *50*, 2509–2522.

(14) Alhumaidan, F.; Cresswell, D.; Garforth, A. Hydrogen storage in liquid organic hydride: Producing hydrogen catalytically from methylcyclohexane. *Energy Fuels* **2011**, *25*, 4217–4234.

(15) Nagatake, S.; Higo, T.; Ogo, S.; Sugiura, Y.; Watanabe, R.; Fukuhara, C.; Sekine, Y. Dehydrogenation of methylcyclohexane over Pt/TiO_2 catalyst. *Catal. Lett.* **2016**, *146*, 54–60.

(16) Chen, C. X.; Cao, J. P.; Jiang, W.; Tang, W.; Zhang, C.; Yao, N. Y.; Wang, H. Y.; Zhao, X. Y. Effect of Pt particle size on methylcyclohexane dehydrogenation over Pt/Al_2O_3 catalysts. *Fuel* **2024**, *360*, No. 130607.

(17) Thybaut, J. W.; Saeys, M.; Marin, G. B. Hydrogenation kinetics of toluene on Pt/ZSM-22. *Chem. Eng. J.* **2002**, *90*, 117–129.

(18) Pushkarev, V. V.; An, K.; Alayoglu, S.; Beaumont, S. K.; Somorjai, G. A. Hydrogenation of benzene and toluene over size controlled Pt/SBA-15 catalysts: Elucidation of the Pt particle size effect on reaction kinetics. *J. Catal.* **2012**, *292*, 64–72.

(19) Auer, F.; Blaumeiser, D.; Bauer, T.; Bösmann, A.; Szesni, N.; Libuda, J.; Wasserscheid, P. Boosting the activity of hydrogen release from liquid organic hydrogen carrier systems by sulfur-additives to Pt on alumina catalysts. *Catal. Sci. Technol.* **2019**, *9*, 3537–3547.

(20) Murata, K.; Onoda, J.; Yamamoto, Y.; Oda, A.; Ohyama, J.; Satsuma, A. Enhancement of toluene hydrogenation activity of supported Pt nanoparticles with increasing the crystallinity of Pt. *Appl. Catal., A* **2022**, *629*, No. 118425.

(21) Zhao, W.; Chizallet, C.; Sautet, P.; Raybaud, P. Dehydrogenation mechanisms of methyl-cyclohexane on γ-Al_2O_3 supported Pt_{13}: Impact of cluster ductility. *J. Catal.* **2019**, *370*, 118–129.

(22) Chen, F.; Huang, Y.; Mi, C.; Wu, K.; Wang, W.; Li, W.; Yang, Y. Density functional theory study on catalytic dehydrogenation of methylcyclohexane on Pt(111). *Int. J. Hydrogen Energy* **2020**, *45*, 6727–6737.

(23) Mi, C.; Huang, Y.; Chen, F.; Wu, K.; Wang, W.; Yang, Y. Density functional theory study on dehydrogenation of methylcyclohexane on Ni–Pt(111). *Int. J. Hydrogen Energy* **2021**, *46*, 875–885.

(24) Onyebuchi Obodo, K.; Naphtaly Moro Ouma, C.; Bessarabov, D. Modified Pt(211) and (311) surfaces towards the dehydrogenation of methylcyclohexane to toluene: A density functional theory study. *Appl. Surf. Sci.* **2022**, *584*, No. 152590.

(25) Kresse, G.; Hafner, J. Ab initio molecular dynamics for liquid metals. *Phys. Rev. B* **1993**, *47*, 558–561.

(26) Kresse, G.; Hafner, J. Ab initio molecular-dynamics simulation of the liquid-metal-amorphous-semiconductor transition in Germanium. *Phys. Rev. B* **1994**, *49*, 14251–14269.

(27) Kresse, G.; Furthmüller, J. Efficiency of ab-initio total energy calculations for metals and semiconductors using a plane-wave basis set. *Comput. Mater. Sci.* **1996**, *6*, 15–50.

(28) Kresse, G.; Furthmüller, J. Efficient iterative schemes for ab initio total-energy calculations using a plane-wave basis set. *Phys. Rev. B* **1996**, *54*, 11169–11186.

(29) Blöchl, P. E. Projector augmented-wave method. *Phys. Rev. B* **1994**, *50*, 17953–17979.

(30) Kresse, G.; Joubert, D. From ultrasoft pseudopotentials to the projector augmented-wave method. *Phys. Rev. B* **1999**, *59*, 1758–1775.

(31) Perdew, J. P.; Burke, K.; Ernzerhof, M. Generalized gradient approximation made simple. *Phys. Rev. Lett.* **1996**, *77*, 3865–3868.

(32) Grimme, S.; Antony, J.; Ehrlich, S.; Krieg, H. A consistent and accurate ab initio parametrization of density functional dispersion correction (DFT-D) for the 94 elements H-Pu. *J. Chem. Phys.* **2010**, *132*, No. 154104.

(33) Henkelman, G.; Uberuaga, B. P.; Jónsson, H. A climbing image nudged elastic band method for finding saddle points and minimum energy paths. *J. Chem. Phys.* **2000**, *113*, 9901–9904.

(34) Momma, K.; Izumi, F. VESTA 3 for three-dimensional visualization of crystal, volumetric and morphology data. *J. Appl. Crystallogr.* **2011**, *44*, 1272–1276.
(35) Hindmarsh, A. C. ODEPACK, A Systemized Collection of ODE Solvers. *Scientific Computing*; North-Holland, **1983**.
(36) Petzold, L. Automatic selection of methods for solving stiff and nonstiff systems of ordinary differential equations. *SIAM J. Sci. Stat. Comput.* **1983**, *4*, 136–148.
(37) Jiang, L. Q.; Koel, B. E. Hydrocarbon trapping and condensation on platinum (111). *J. Phys. Chem.* **1992**, *96*, 8694–8697.
(38) Ihm, H.; Ajo, H. M.; Gottfried, J. M.; Bera, P.; Campbell, C. T. Calorimetric measurement of the heat of adsorption of benzene on Pt(111). *J. Phys. Chem. B* **2004**, *108*, 14627–14633.
(39) Gottfried, J. M.; Vestergaard, E. K.; Bera, P.; Campbell, C. T. Heat of adsorption of naphthalene on Pt(111) measured by adsorption calorimetry. *J. Phys. Chem. B* **2006**, *110*, 17539–17545.
(40) Chorkendorff, I.; Niemantsverdriet, J. W. *Concepts of Modern Catalysis and Kinetics*, rd ed.; Wiley-VCH: Weinheim, **2017**.
(41) Linstrom, P. J.; Mallard, W. G. *NIST Chemistry WebBook*, NIST Standard Reference Database Number 69; National Institute of Standards and Technology: Gaithersburg, MD, **2005**. http://webbook.nist.gov [Online] (accessed Dec 11, 2020).
(42) Delley, B. An all-electron numerical method for solving the local density functional for polyatomic molecules. *J. Chem. Phys.* **1990**, *92*, 508–517.
(43) Delley, B. From molecules to solids with the $DMol^3$ approach. *J. Chem. Phys.* **2000**, *113*, 7756–7764.
(44) BIOVIA, Dassault Systèmes Materials Studio, *$DMol^3$ Module Used for Calculations*, version 2020; Dassault Systèmes: San Diego, CA, **2020**.
(45) Eyring, H. The activated complex in chemical reactions. *J. Chem. Phys.* **1935**, *3*, 107–115.
(46) Campbell, C. T. The degree of rate control: A powerful tool for catalysis research. *ACS Catal.* **2017**, *7*, 2770–2779.
(47) Blaylock, D. W.; Ogura, T.; Green, W. H.; Beran, G. J. O. Computational investigation of thermochemistry and kinetics of steam methane reforming on Ni(111) under realistic conditions. *J. Phys. Chem. C* **2009**, *113*, 4898–4908.
(48) Peterson, A. A.; Abild-Pedersen, F.; Studt, F.; Rossmeisl, J.; Nørskov, J. K. How copper catalyzes the electroreduction of carbon dioxide into hydrocarbon fuels. *Energy Environ. Sci.* **2010**, *3*, 1311–1315.
(49) Granda-Marulanda, L. P.; Rendón-Calle, A.; Builes, S.; Illas, F.; Koper, M. T. M.; Calle-Vallejo, F. A semiempirical method to detect and correct DFT-based gas-phase errors and its application in electrocatalysis. *ACS Catal.* **2020**, *10*, 6900–6907.
(50) Posada-Borbón, A.; Grönbeck, H. A first-principles-based microkinetic study of CO_2 reduction to CH_3OH over In_2O_3(110). *ACS Catal.* **2021**, *11*, 9996–10006.
(51) Manabe, S.; Yabe, T.; Nakano, A.; Nagatake, S.; Higo, T.; Ogo, S.; Nakai, H.; Sekine, Y. Theoretical investigation on structural effects of Pt–Mn catalyst on activity and selectivity for methylcyclohexane dehydrogenation. *Chem. Phys. Lett.* **2018**, *711*, 73–76.
(52) El-Sawi, M.; Infortuna, F. A.; Lignola, P. G.; Parmaliana, A.; Frusteri, F.; Giordano, N. Parameter estimation in the kinetic model of methylcyclohexane dehydrogenation on a Pt—Al_2O_3 catalyst by sequential experiment design. *Chem. Eng. J.* **1989**, *42*, 137–144.
(53) Wang, J.; Li, P.; Wang, S.; Lu, S.; Shi, Q.; Wang, B.; Gong, X.; Yang, F.; Fang, T. Modelling and kinetics of the toluene/methylcyclohexane-based hydrogen storage system. *Can. J. Chem. Eng.* **2025**, *103*, 3877–3887.

https://doi.org/10.1021/acscatal.6c01477
ACS Catal. 2026, 16, 12123–12134